Monitoring Ras Interactions with the Nucleotide Exchange Factor Sos using Site-specific NMR Reporter Signals and Intrinsic Fluorescence

DOI:
10.1074/jbc.M115.691238

Document Version
Final published version

Published in:
Journal of Biological Chemistry (Online)

JBC Papers in Press. Published on November 12, 2015 as Manuscript M115.691238
The latest version is at http://www.jbc.org/cgi/doi/10.1074/jbc.M115.691238

Monitoring Ras Interactions with the Nucleotide Exchange Factor Sos using Site-specific NMR Reporter Signals and Intrinsic Fluorescence

Uybach Vo[‡], Navratna Vajpai[§], Liz Flavell[§], Romel Bobby[§], Alexander L. Breeze[§,1], Kevin J. Embrey[§,2], and Alexander P. Golovanov [‡,2]

From [‡] Manchester Institute of Biotechnology and Faculty of Life Sciences, The University of Manchester, 131 Princess Street, Manchester M1 7DN, UK, and

[§] AstraZeneca, Discovery Sciences, Mereside, Alderley Park, Cheshire, SK10 4TF, UK

[1] Present address: Astbury Centre for Structural Molecular Biology, School of Molecular and Cellular Biology, University of Leeds, Leeds, LS2 9JT, UK
[2] To whom correspondence should be addressed: Alexander P. Golovanov, Manchester Institute of Biotechnology and Faculty of Life Sciences, The University of Manchester, 131 Princess Street, Manchester M1 7DN, UK, Tel.: +441613065813; Fax: +441613065201; E-mail: A.Golovanov@manchester.ac.uk; and
Kevin J. Embrey, AstraZeneca, Discovery Sciences, Mereside, Alderley Park, Cheshire, SK10 4TF, UK, Tel.: +441625518659, E-mail: Kevin.Embrey@astrazeneca.com

Running title: *Monitoring Ras:Sos interactions*

Keywords: Allosteric regulation; Nuclear Magnetic Resonance (NMR); protein-protein interactions; Ras protein; small GTPase; Sos protein.

ABSTRACT

The activity of Ras is controlled by the inter-conversion between GTP- and GDP-bound forms, partly regulated by the binding of the guanine nucleotide exchange factor Son of Sevenless (Sos). The details of Sos binding, leading to nucleotide exchange and subsequent dissociation of the complex, are not completely understood. Here, we used uniformly [^{15}N]-labeled Ras, as well as [^{13}C-methyl-M,I]-labeled Sos, for observing site-specific details of Ras:Sos interactions in solution. Binding of various forms of Ras (loaded with GDP and mimics of GTP, or nucleotide-free) at the allosteric and catalytic sites of Sos was comprehensively characterized, by monitoring signal perturbations in the NMR spectra. The overall affinity of binding between these protein variants, as well as their selected functional mutants, was also investigated using intrinsic fluorescence. The data supports a positive feedback activation of Sos by Ras•GTP, with Ras•GTP binding as a substrate for the catalytic site of activated Sos more weakly than Ras•GDP, suggesting that Sos should actively promote unidirectional GDP→GTP exchange on Ras, in preference of passive homonucleotide exchange. Ras•GDP weakly binds to the catalytic, but not to the allosteric site of Sos. This confirms that Ras•GDP cannot properly activate Sos at the allosteric site. The novel site-specific assay described may be useful for design of drugs aimed at perturbing Ras:Sos interactions.

Ras proteins are mutated in 30% of all human tumors, contributing to several malignant phenotypes including abnormal cell growth, proliferation and apoptosis (1). The activity of Ras is controlled by the inter-conversion between GTP- and GDP- bound forms, with GTP-binding required for the active form (2). Ras activation is mediated through the binding of guanine nucleotide exchange factors (GEFs), of which the most important is Son of Sevenless (Sos), which stimulates the release of bound GDP from Ras and is currently thought to facilitate the more abundant cytosolic GTP to bind in its place (3). The major Ras isoforms, H-Ras, K-Ras and N-Ras, are closely related, bearing 85% amino acid sequence identity; however, 85% of clinically-observed Ras

mutations occur in K-Ras (4). Point mutations at codon 12 impair the GTPase activity of Ras isoforms, both by preventing productive binding of GTPase activating proteins (GAPs) that accelerate GTP hydrolysis and by suppressing intrinsic (basal) GTP hydrolase activity. The single-point mutation of G12V in K-Ras, which is a common variant found in human tumors, causes constitutive activation of Ras (5). This leads to an accumulation of the GTP-bound active form of K-Ras (6).

Over the last few decades, studies have shown that several regions of Ras are of particular interest for control of its functional cycle and present potential intervention sites for new therapeutics (4-7). The P-loop (residues G10–S17) is responsible for phosphate binding, while the Switch I (Y32–Y40) and Switch II (G60–T75) regions are critical for interactions with GEFs (7) and effector proteins (8). Sos contains two domains that are essential for Ras-nucleotide exchange, namely the Ras-exchanger motif (REM) domain, and the Cdc25 domain. The latter contains the catalytic site in which bound Ras undergoes nucleotide exchange (9,10). A second Ras molecule binds at a distal (also called allosteric) site, which is located between the REM and Cdc25 domains. Binding of Ras•GTP to the allosteric site induces a conformational change that is propagated to the catalytic site (10-12), enhancing the rate of Ras nucleotide exchange activity by increasing the affinity of Ras at the catalytic site. However, it remains unclear whether or to what extent GDP-loaded Ras can allosterically activate Sos (11-13), and whether different forms of Ras bind at the catalytic site of activated Sos equally well. One current model is that weak binding of Ras•GDP at the distal (allosteric) site causes basal activation of Sos for further catalytic site binding (11), with stronger Ras•GTP binding at the distal site promoting a significantly higher level of activation, resulting in a positive feedback activation mechanism (10-12). Additionally, the binding at the allosteric site (and hence the activation of Sos) is regulated and auto-inhibited by interactions with neighboring histone, Dbl homology (DH) and pleckstrin homology (PH) domains of Sos (11,14).

Currently, nucleotide exchange at the catalytic site is presumed to be passive: GDP is exchanged for GTP driven through the higher cytosolic concentration of GTP (3). For convenience, currently used nucleotide exchange assays often quantify the homonucleotide exchange, GDP→GDP or GTP→GTP, as a measure of biological activity of Sos (10,11,13). It is however unclear whether or how rebinding of GDP or GTP to nucleotide-free Ras (a presumed transition state) at the catalytic site of Sos occurs and how this triggers the dissociation of Ras upon completion of nucleotide exchange, allowing Sos to engage in further cycles of GEF activity. Binding of Ras•GTP at the allosteric site and thus activating Sos increases affinity of Ras•GDP binding at the catalytic site, with a measured K_d of 1.9 μM (11), but, to our knowledge, the affinity of Ras•GTP binding to the catalytic site of activated Sos has not been reported to date.

The model of Sos activation by binding of Ras to the allosteric site is based on static snap-shots from X-ray crystal structures (10,11) and therefore may not fully represent the dynamic subtleties of the process in solution. Indeed, recent single-molecule studies have suggested a critical role for dynamic fluctuations in the allosteric activation of Sos by Ras•GTP, and also hinted at the possibility that Ras•GDP can also activate Sos (13). How these fluctuations are modulated at a detailed structural level, and whether Ras•GDP can bind with sufficient affinity to the allosteric site to activate Sos remains to be established.

Previous solution NMR studies, which can capture the dynamic behavior of proteins, have explored the process of GTP hydrolysis and nucleotide exchange in H-Ras (15-17). Other studies were able to demonstrate that H-Ras interacts with its downstream effector proteins, such as Raf kinases (18-20). Studies using ^{31}P NMR spectroscopy revealed that the GTP-bound form of Ras is likely to exist in two or more conformational states, interconverting on the millisecond timescale (21). The conformational equilibrium can be shifted by introducing point mutations that enhance the affinity of GTP-Ras for Raf kinases (21-25).

To our knowledge, no detailed solution studies of the Ras:Sos interactions using NMR spectroscopy have yet been reported. Here we use NMR to dissect Ras:Sos interactions. Signal perturbations were employed to monitor changes in Ras and Sos upon binding, depending on their stoichiometry and type of nucleotide present.

Moreover, we introduced a number of non-perturbing probes (^{13}C-labeled methyls of methionines (26)) into Sos and used them to monitor Ras binding separately to the allosteric and catalytic sites. Using intrinsic fluorescence, we have also measured the binding affinity to Sos of wild-type (WT) as well as functional mutants of Ras in various nucleotide-loaded forms. Our data have enabled us to disentangle the binding preferences of GTP and GDP-loaded forms of Ras in solution at the specific sites on Sos.

EXPERIMENTAL PROCEDURES

Protein expression and purification- H-Ras (residues 1-166), K-Ras (1-166), Sos^{Cat} (563-1049) and Sos$^{HD\text{-}DH\text{-}PH\text{-}Cat}$ (1-1049) gene sequences were synthesized by Geneart (Life Technologies) and cloned into a pET28b vector, with an N-terminal His_6-tag followed by a TEV cleavage site prior to the protein sequence. Proteins were expressed in BL21-GOLD(DE3) competent cells and the seeder cultures were grown in Luria Broth (LB) medium. All samples were grown using a similar protocol (27) for unlabeled and uniformly ^{15}N-labeled H-Ras samples. WT and mutant Sos constructs (Sos^{Cat} and Sos$^{HD\text{-}DH\text{-}PH\text{-}Cat}$) were grown in minimal M9 media containing 50 μg/mL of Kanamycin and 12.5 μg/mL of Tetracycline antibiotics, supplemented with micronutrients and vitamins. Cells were then induced by 0.1 mM of IPTG (Isopropyl β-D-1-thiogalactopyranoside) followed by the addition of 2 g/L D-glucose. Uniformly ^{13}C-labeled at the Met (ϵ-) and Ile (δ_1-) methyl positions recombinant Sos^{Cat} ([^{13}C-methyl-M,I]-Sos^{Cat}) was produced under a similar protocol in D_2O but with an additional feed of 200 mg/L of ^{13}C-methyl Met, 120 mg/L of ^{13}C-methyl α-keto butyrate and 2g/L of d7-D-Glucose administered at the point of IPTG induction. Protein purification was carried out as previously described (27). Unless stated otherwise, all proteins were cleaved from their N-terminal His_6-tags using TEV protease.

Nucleotide exchange in Ras samples- Purified H-Ras samples were incubated with 20 fold excess of GTPγS (guanosine-5′-[γ-thio]-triphosphate), GppNp (guanosine-5′-[(β,γ)-imino]-triphosphate) or GppCp (guanosine-5′-[(β,γ)-methyleno]-triphosphate) and 1/100 fold of His-tagged Sos in 50 mM Hepes, 50 mM NaCl, 2 mM $MgCl_2$, 2 mM TCEP, 0.1 mM EDTA, 0.02 % NaN_3 at pH 7.4. The samples were left overnight at 4 °C to allow nucleotide exchange. The mixture was then passed through a Ni-NTA column equilibrated with 30 mM Na_2HPO_4, 1mM DTT, 2 mM $MgCl_2$ and 0.1 mM EDTA, 0.02% NaN_3 at pH 7.0 to remove the His_6-tagged Sos and free nucleotide. The samples were concentrated using 0.5 mL VivaSpin concentrators (Sartorius, 10,000 MWCO). Protein concentration was determined by standard Bradford assays. Nucleotide exchange was confirmed by electrospray mass spectrometry. For the preparation of the nucleotide-free state of Ras (hereafter referred to as H-Ras^{NF}), H-Ras•GDP (200 μM) sample was incubated with 20 mM EDTA to strip the Mg^{2+} and nucleotide from Ras. After 2 hours, the sample was passed down a pre-equilibrated Nap-5 column (GE healthcare) to exchange the sample into Hepes buffer pH 7.4 containing 50 mM of L-Arg and L-Glu to improve sample stability for the duration of NMR measurements (28). H-Ras^{NF} was then concentrated down as required using an Amicon Ultra-15 centrifugal filter unit (Millipore) with a 10,000 MWCO.

NMR experiments- All NMR spectra were collected at 298 K (unless stated otherwise) on Bruker 600 and 800 MHz (Avance I and III, respectively) spectrometers equipped with 5 mm TCI Cryoprobes with Z-axis gradients using standard experiments and parameters from Bruker library. Uniformly ^{15}N-labeled H-Ras was used at a concentration of 100 μM, and [^{13}C-methyl-M,I]-Sos^{Cat} at 60 μM, with concentrations of added non-labeled protein variants as indicated. NMR samples containing proteins or their mixtures were prepared in either phosphate buffer at pH 7.0 or Hepes buffer at pH 7.4 supplemented with 5% D_2O, and placed in a Shigemi tube. All spectra were processed in Topspin 2.1 or 3.1 and analyzed in NMRViewJ (29).

Measuring affinities of Ras:Sos interactions- Fluorescence binding assays were performed using a Luminescence spectrometer (Perkin-Elmer) with emission and excitation slits set to 3 nm and 10 nm, respectively. Samples were measured in 1 mL quartz cuvettes with path lengths of 1 cm and 0.4 cm, used for excitation (295 nm) and emission (336 nm), respectively. Data points were taken in quadruplicate with a scan speed of 300 ns/min. WT Sos^{Cat} or Sos$^{HD\text{-}DH\text{-}PH\text{-}Cat}$ samples (10 μM) were incubated with increasing amounts of Ras (1 - 50

μM) in Hepes buffer. To obtain the dissociation constant of binding (K_d), the quenching of intrinsic fluorescence of the Trp residues in Sos, upon addition of the non-fluorescent Ras protein, was monitored. The weak contribution of intrinsic fluorescence of Ras, as well as change in fluorescence due to dilution effects were taken into account and compensated for. Fluorescence experiments were repeated three times. Data points were fitted (change in fluorescence versus Ras concentration) using non-linear regression to a standard quadratic binding equation using GraFit (30).

RESULTS

Fluorescence measurements -

The overall apparent binding affinities of Ras to Sos were determined by monitoring the change (ie, quenching) in Sos fluorescence upon the formation of the Ras:Sos complex (Figure 1). This approach relied on the strong intrinsic fluorescence signal of the multiple Trp residues within the Sos^{Cat} and $Sos^{HD\text{-}DH\text{-}PH\text{-}Cat}$. Ras is devoid of Trp residues and therefore its intrinsic fluorescence signal at 295 nm is negligible. To determine the affinities accurately, the minor dilution effect and the background fluorescence of Ras (without Sos) were further subtracted from the overall fluorescence. First, we explored the differences in binding of the isoforms, H-Ras and K-Ras, as well as K-RasG12V, a common cancer-associated mutant, to Sos when Ras was loaded with different stable analogues of GTP. Traditionally, nucleotide exchange has been studied using fluorescently labeled analogues such as mant•GTP (2′/3′-O-(N-methylanthraniloyl guanosine 5'-[gamma-thio] triphosphate) (11,14,31); however, the bulky mant adduct has been shown to affect the kinetics of nucleotide exchange and hydrolysis in H-Ras (16,23). For these reasons, we employed unlabeled slowly- or non- hydrolysable GTP mimics (GTPγS, GppNp and GppCp) in our study, coupled with measurement of intrinsic protein fluorescence. Dissociation constants (K_d) for interactions of H-Ras•GTPγS, H-Ras•GppNp and H-Ras•GppCp with Sos^{Cat} are generally very similar to each other (~5-8 μM) (Table 1). Conversely, the affinity of H-Ras•GDP for Sos^{Cat} is approximately ten-fold weaker (K_d ~54 μM) (Table 1). These results are in agreement with the affinities previously measured for Ras•GDP binding at the allosteric site of non-activated Sos (11). In addition, the binding of K-Ras•GTPγS to Sos^{Cat} (K_d = 10 ± 1 μM) is stronger than K-RasG12V•GTPγS (K_d = 31 ± 2 μM), but comparable to binding affinities of H-Ras loaded with GTP analogs (Table 1). This suggests that WT K-Ras and H-Ras have fairly similar Sos binding properties, whereas the oncogenic mutation K-RasG12V has reduced binding affinity to Sos.

To assess the affinity of Ras binding specifically at the catalytic site of Sos (when Sos is not activated), we set up further experiments so that the allosteric site of Sos was either obstructed, as in the $Sos^{HD\text{-}DH\text{-}PH\text{-}Cat}$ variant, or disrupted by mutation, as in Sos^{Cat}W729E (10-12,14,32,33). The affinity of H-Ras•GTPγS for $Sos^{HD\text{-}DH\text{-}PH\text{-}Cat}$ (K_d = 24 μM) and for Sos^{Cat}W729E (K_d = 28 μM) is significantly weaker than H-Ras•GTPγS binding to WT Sos^{Cat} (K_d = 5 μM, Table 1). The binding of H-Ras•GDP to Sos^{Cat}W729E (K_d = 67 μM) is weaker than the binding of H-Ras•GTP to the same construct (Table 1).

Interestingly, when the allosteric site of Sos^{Cat} is partially saturated by the addition of excess H-RasY64A•GTPγS, a mutant which cannot bind to the catalytic site of Sos (11), the fluorescence measurements reveal that the binding of WT H-Ras•GTPγS at the catalytic site is weak with an observed K_d of 21 μM (Table 1). This figure provides an upper limit estimate for the binding affinity to the catalytic site, as much of the observed affinity may be due to competition between the Ras forms for the allosteric site. Although the addition of RasY64A•GTPγS in this experiment was expected to activate Sos for further catalytic site binding (11,12), our results suggest H-Ras•GTPgS has only a modest-to-weak affinity ($K_d \geq$ 21 μM) for the catalytic site of Sos. This result complements earlier studies in which loading of H-RasY64A•GppNp at the allosteric site was found to increase the affinity for Ras•GDP at the catalytic site, with a K_d of 1.9 μM (11). GppNp is another analog of GTP, with functional properties similar to those of GTPγS (see Table 1). The weaker binding observed for Ras•GTP at the catalytic site have not been described previously and is significant, as it implies that Ras•GTP-activated Sos preferentially binds Ras•GDP at its catalytic site, but not Ras•GTP. This suggests a clear preference of activated Sos for the heteronucleotide exchange reaction GDP→GTP at

its catalytic site, which we believe has not been previously recognized.

The binding of mutant H-RasY64A (K_d = 10 μM) to Sos^{Cat} was marginally weaker but comparable to WT H-Ras, suggesting that this mutant and the wild-type protein have similar binding properties when they are loaded with GTPγS, and both of them preferentially bind to the allosteric site. Attempts to fit the quantitative binding data to a two-site model found no significant improvement in the fit over the simpler one-site models and is in agreement with Ras•GTPγS preferentially interacting at only one, namely the allosteric, site. To study the site-specific binding of Ras with Sos further, we monitored these interactions using NMR spectroscopy.

Monitoring NMR signal perturbations of H-Ras upon binding to different nucleotides and Sos. First, the previous $^{1}H^{N}$ and ^{15}N backbone assignments of Ras residues 1-166 (17,27) were transferred to spectra of nucleotide-loaded and nucleotide-free states to achieve their partial assignment for a number of signals used as reporters. Amide signal perturbations of the GDP- and GTP-bound forms of uniformly ^{15}N-labeled H-Ras were then monitored by acquiring $^{1}H,^{15}N$-correlation TROSY spectra upon the addition of unlabeled Sos^{Cat} (Figure 2). The influence of the nucleotide in maintaining the structural integrity of H-Ras was also investigated by comparing the spectra of the nucleotide-free form of H-Ras ($H\text{-}Ras^{NF}$) with the nucleotide-loaded forms, H-Ras•GDP and H-Ras•GTPγS (Figure 2).

The addition of unlabeled WT Sos^{Cat} to the ^{15}N-labeled $H\text{-}Ras^{NF}$ sample at a stoichiometry of 2:1 (Ras:Sos) showed clear signal perturbations for a number of Ras residues and the re-appearance of two amide peaks belonging to residues C118 and T124 (Figure 3A). These signals which became somewhat broadened for unbound nucleotide-free Ras^{NF}, recovered for Ras^{NF} bound to Sos, in positions similar to the GDP-loaded form. The chemical shifts were generally comparable to those caused by GDP binding to $H\text{-}Ras^{NF}$. Overall, this result confirms that $H\text{-}Ras^{NF}$ and Sos are able to form a complex in solution, and this binding affects Ras dynamics. Our observations are thus consistent with a model whereby binding of Ras at the catalytic site of Sos stabilizes its nucleotide-free conformation, and primes it for reloading with GTP (8,10).

Intriguingly, from our signal perturbation study, it is clear that addition of Sos^{Cat} to ^{15}N-labeled H-Ras•GDP does not induce any noticeable changes in its $^{1}H,^{15}N$-correlation spectrum, with no noticeable effects on peak positions or line widths (Figure 3B), suggesting that this interaction is very weak, and much weaker than the interaction with $H\text{-}Ras^{NF}$. The K_d of H-Ras•GDP binding with Sos^{Cat} measured by fluorescence is only 54 μM (Table 1). Our solution NMR data corroborate previous findings that basal binding of Ras•GDP with Sos at either site is relatively weak, and would require binding of Ras•GTP at the allosteric site to increase the affinity of Sos for Ras•GDP at the catalytic site (10,11). This Ras•GDP binding contrasts with Ras^{NF}, which can bind to Sos directly, even in the absence of Ras•GTP (8).

The addition of unlabeled Sos^{Cat} to a ^{15}N-labeled H-Ras•GTPγS sample at a 2:1 Ras:Sos stoichiometry revealed some significant changes in the TROSY spectrum (Figure 3C). This provides evidence that H-Ras•GTPγS is able to bind to Sos with higher affinity than H-Ras•GDP, and that this increased affinity is accompanied by significant structural and/or dynamic rearrangements for H-Ras. A closer analysis of the signal shift patterns in the NMR spectra of the complexes of Ras with GDP, GTPγS and GTPγS+Sos revealed that change of GDP for GTP causes significant chemical shift changes for a number of residues, such as Q25, C118, T124 and S145, whereas subsequent binding of Sos to Ras•GTPγS shifts its peaks back to positions similar to those in the free Ras•GDP (Figure 3C). This intriguing observation is difficult to explain definitively based on available measurements: due to the presence of two different binding sites for Ras on Sos^{Cat}, it is not clear whether these signal changes are characteristic of conformational change upon Ras binding at the allosteric or catalytic sites, and/or exchange between the two. Further experiments, e.g., using pre-loading with H-RasY64A•GTPγS, a mutant which can only bind to the allosteric site, or using different ratios of components, as well as using ^{31}P NMR spectroscopy (21-25), may provide an explanation in the future.

The NMR data presented here clearly show that different forms of Ras, either nucleotide-free or loaded with GDP or GTP, bind Sos with different affinities, causing some characteristic changes in the TROSY spectra of Ras. However, as the P-loop, Switch I and II regions of Ras are structurally shown to be involved in binding at both catalytic and allosteric sites of Sos (10), it remains challenging to distinguish effects of binding at these two sites when observing the signal perturbations of Ras only. Therefore, in order to gain better insight into the site-specific interactions of Ras with Sos, we have monitored the formation of the same complexes using unlabeled Ras and ^{13}C-methyl Met, Ile-labeled Sos^{Cat}.

^{13}C–methyl Met resonance assignment of Sos^{Cat}. To monitor Ras binding at the allosteric and catalytic sites of Sos, we recorded 2D ^{1}H,^{13}C-HMQC spectra of a sample of Sos^{Cat} (60 μM) that was uniformly ^{13}C-labeled (34) at the Met (ε-) and Ile (δ_1-) methyl positions (that we call for brevity [^{13}C-methyl-M,I]-Sos^{Cat}). The methyl resonances from ten labeled Met residues occurring in Sos^{Cat} are well resolved (Figure 4A), whereas the methyls from thirty nine Ile residues suffer from significant spectral overlap in the HMQC spectra (Figure 4B). Therefore, we focused on methyl-Met signals. To obtain the methyl resonance assignments, we consecutively substituted Ala for Met, creating ten mutant forms of Ras: M563A, M567A, M592A, M617A, M714A, M726A, M824A, M878A, M997A and M1001A. The absence of methyl signal in the spectrum of the mutant allows the assignment for this methionine in the spectrum of the WT protein (Figure 5A,B). Through this comprehensive mutagenesis approach, eight of the ten Met methyl signals were unambiguously assigned (Figure 4A). The spectra of M567A and M997A yielded no clear changes relative to the WT spectrum, which, with one unassigned peak remaining, suggest that the methyl signals from these two residues overlap with each other and both contribute to this remaining unassigned peak.

Mapping the position of Met residues onto the crystal structure of the Ras:Sos complex (10) and relating them to positions of allosteric and catalytic binding sites (Figure 4C, Figure 5C,D), it is possible to separate signals into groups, as originating from (and presumably, primarily reporting on) allosteric (a) and catalytic (c) sites. A third group of Met residues is positioned in-between the sites (a/c) and thus may report on structural changes in Sos in response to binding at either of these sites. For convenience, we will indicate the site-specific origin of these potential reporter signals with corresponding superscripts, with M563$^{(a)}$, M592$^{(a)}$, M617$^{(a)}$ and M726$^{(a)}$ arising from the allosteric site of Sos, and residues M824$^{(c)}$, M878$^{(c)}$ and M1001$^{(c)}$ arising from the catalytic site. M714$^{(a/c)}$ is positioned in between the allosteric and catalytic sites and therefore belongs to the third group. Subsequent titration experiments (see below) showed that in fact only three of these potential reporters, M726$^{(a)}$, M824$^{(c)}$ and M714$^{(a/c)}$, display appreciable sensitivity to Ras binding at the allosteric and catalytic sites.

Monitoring NMR signal perturbations of Sos^{Cat} upon addition of H-Ras^{NF}. To investigate the binding of Sos^{Cat} to nucleotide-free H-Ras, increasing amounts of unlabeled H-Ras^{NF} were added to a sample containing [^{13}C-methyl-M,I]-Sos^{Cat} (Figure 6A). The addition of H-Ras^{NF} at higher concentrations, e.g. above 2:1 Ras:Sos stoichiometry, showed severe broadening for the M824$^{(c)}$ resonance (Figure 6A), suggesting that H-Ras^{NF} binds at the catalytic site of Sos^{Cat}. Furthermore, slight signal broadening was also observed for M714$^{(a)/(c)}$. Residue M714$^{(a)/(c)}$ is located near the core of Sos and is therefore possibly sensitive to the conformational and/or dynamic changes induced in Sos upon H-Ras^{NF} binding. Most importantly, residue M726$^{(a)}$ (which turned out to be the most sensitive probe for binding at the allosteric site, see below) was largely unperturbed, suggesting that H-Ras^{NF} does not bind at the allosteric site. Our site-specific results therefore indicate that H-Ras^{NF} in solution can only bind to the catalytic site of Sos. This complements previous crystal studies of H-Ras and Sos (8,10), which showed nucleotide-free H-Ras ever bound at the catalytic site only.

Monitoring signal perturbations of Sos^{Cat} upon H-Ras•GDP binding. Binding of Ras•GDP to Sos promotes a basal level of nucleotide exchange activity which is observed in GDP→GDP exchange assays (11-13). Ras•GDP binding to the allosteric site is believed to induce weak

nucleotide-exchange activity at the catalytic site (11). Here, we explored directly to which of the sites H-Ras•GDP binds, by adding unlabeled Ras•GDP to [^{13}C-methyl-M,I]-Sos^{Cat}. The methyl signals of Sos M714$^{(a/c)}$ and M824$^{(c)}$ are heavily broadened in the HMQC spectra of 2:1 and 4:1 H-Ras•GDP:Sos samples, whereas these signals are still visible in the spectrum of a 1:1 H-Ras•GDP:Sos sample (Figure 6B). Signal broadening of M714$^{(a/c)}$ in Sos indicates that H-Ras•GDP may cause some conformational or dynamical changes to Sos. Interestingly, M726$^{(a)}$ was not significantly perturbed, even at 4-fold excess of H-Ras•GDP, suggesting that Ras•GDP does not associate noticeably with the allosteric site of Sos^{Cat}. Importantly, the broadening of M824$^{(c)}$ signal confirms that H-Ras•GDP binds to the catalytic site (Figure 6B), suggesting that binding to the catalytic site can occur in the absence of significant occupancy of the allosteric site. Overall, the binding is relatively weak, in agreement with our other NMR (Figure 3B) and fluorescence data (Table 1). Preferential weak binding of H-Ras•GDP to the catalytic site of Sos, but not to the allosteric site, suggests that H-Ras•GDP is not expected to play a significant role in activating Sos via allosteric interactions, and that the basal, low-level activity of Sos for GDP→GDP exchange in the absence of GTP may be due to inherent weak binding of Ras•GDP to the catalytic site only. The role of DH-PH and histone domains of Sos (11,32) in further down-regulating its basal catalytic activity thus may be more subtle than just sterically blocking the allosteric site for Ras•GDP (as well as for Ras•GTP) binding.

Monitoring signal perturbations of Sos^{Cat} upon H-Ras•GTPγS binding. Ras•GTP binding to the allosteric site of Sos is expected to lead to Sos activation (10), whereas the ability of Ras•GTP to bind at the catalytic site of activated Sos has always been implied in the GTP→GTP exchange assays (11,13). However, to our knowledge, the latter assumption has not been tested before. Here, binding between Ras•GTP and Sos was monitored in a site-specific manner, via the HMQC spectra of [^{13}C-methyl-M,I]-Sos^{Cat} upon addition of unlabeled H-Ras•GTPγS. The signals from M726$^{(a)}$, M824$^{(c)}$ and, to a smaller extent, M714$^{(a/c)}$ shifted in the spectra (Figure 6C). Residue M726 from the allosteric site exhibited the largest chemical shift change. In the crystal structure of the complex the side chain of Sos M726$^{(a)}$ is located close to residues I36 and E37 from the Switch I region and Y64 from the Switch II region of H-Ras (Figure 5D). Residues M714$^{(a/c)}$ and M824$^{(c)}$ also showed significant signal perturbations and complex signal movement, occurring simultaneously with perturbations at the allosteric site. Interestingly, close inspection of the M824$^{(c)}$ peak changes during the titration (Figure 6C and Figure 7A) reveals that at 1:1 ratio there are two M824$^{(c)}$ signals observed in slow exchange between State I (free form) and State II (remodeled form); with further addition of H-Ras•GTPγS the State I disappears, and the signal is gradually shifted from State II towards State III (fully-bound), where it remains stable even at higher protein ratios. This peak movement suggests the existence of complex dynamic and structural rearrangements at the catalytic site in response to initial binding at the allosteric site. While, overall, the initial perturbation to M824$^{(c)}$ appears to be dominated by conformational changes in response to binding at the allosteric site, further gradual signal shifts reveal there may be secondary, weaker binding occurring for Ras•GTP at the catalytic site that is in the fast exchange regime on the chemical shift time scale. Our fluorescence experiments, where binding to the allosteric site was partially saturated with the addition of H-RasY64A•GTPγS (Table 1) concurred with only weak binding of H-Ras•GTPγS at the catalytic site. In addition to the shift changes observed on the ^{13}C-methyl of Met, several of the non-assigned ^{13}C-methyl Ile resonances were also significantly perturbed in the presence of H-Ras•GTPγS (data not shown). The complex peak movements observed here, and the presence of both slow and fast chemical exchange regimes, may limit the reliability of signal shifts as a measure of the fraction of protein bound to the ligand (35), which would complicate estimates of K_d's from these signal shifts. Indeed, we could not obtain a good fit for the dependence of signal shifts on concentration to a single-site binding model, neither for allosteric nor for catalytic site signals. Moreover, due to low protein concentrations used here, and the large size of Sos^{Cat} itself and its complexes with H-Ras, the signal-to-noise ratio was too poor to quantify

signal intensities of methyl signals throughout the titration (Figure 7A), which otherwise could have been used to characterize the exchange regimes further. We have however run simulations (Figure 7B-D) which show that signal shift behavior for M824$^{(c)}$ signal can be reasonably recreated for a two-binding-site model with slow and fast exchange regimes. More accurate measurements at much higher protein concentrations, and with more experimental points, would be required to extract qualitative information about the exchange rates in this system. Taken together, the observations by NMR and fluorescence suggest that the overall binding of H-Ras•GTPγS to Sos^{Cat} is dominated by binding at the allosteric site, and its binding to the catalytic site is much weaker than to the allosteric site.

Monitoring signal perturbations of Sos^{Cat} upon K-Ras•GTPγS binding. To explore whether K-Ras binding to Sos differs from that of H-Ras, we titrated unlabeled K-Ras•GTPγS into ^{13}C-methyl I,M-labeled Sos^{Cat}. The signals from M714$^{(a)/(c)}$, M726$^{(a)}$ and M824$^{(c)}$ showed the most significant changes in the spectrum (Figure 6D). In addition to the shift changes observed on the ^{13}C-methyl of Met, several of the ^{13}C-methyl Ile residues were also significantly perturbed in the presence of K-Ras•GTPγS (data not shown). The pattern of perturbation is comparable to that caused by H-Ras•GTPγS. However, the slow conformational exchange observed at the catalytic site in response to occupation of the allosteric site by H-Ras was not detected for K-Ras binding, suggesting that there may be subtle differences in how these Ras isoforms affect the dynamics of Sos, and/or slight differences in binding site affinities. The apparent microscopic K_d value (ca 2 μM) estimated from M726$^{(a)}$ signal shift, which represents K-Ras•GTPγS binding at the allosteric site, is much lower than the apparent macroscopic K_d measured by fluorescence for K-Ras binding to Sos^{Cat} with the assumption of single-site binding model (Table 1), again suggesting that binding at the allosteric site dominates the binding at low ligand concentrations. Since the chemical shift changes follow the same pattern upon H-Ras•GTPγS or K-Ras•GTPγS addition to Sos^{Cat}, it is likely that Sos^{Cat} adopts a similar conformation, albeit accompanied by subtly different dynamic perturbations.

Monitoring signal perturbations in Sos^{Cat} upon K-RasG12V•GTPγS binding. To examine if the binding of the K-RasG12V mutant to Sos^{Cat} is different in any way from its wild-type variant, we recorded HMQC spectra of [^{13}C-methyl-M,I]-Sos^{Cat} upon the addition of unlabeled K-RasG12V•GTPγS. M824$^{(c)}$ signal in the catalytic site of Sos^{Cat} undergoes only a minor shift, but does decrease in intensity and broaden when above equimolar concentrations of K-Ras are added (Figure 6E). The signal perturbations for M726$^{(a)}$ in the allosteric site are less pronounced than observed with WT K-Ras, indicating that binding to the allosteric site of Sos is weaker, for the Ras mutant (Figure 6E). These findings are supported by the binding measurements obtained from our fluorescence studies, which revealed the affinity for K-Ras(G12V)•GTPγS binding to Sos (K_d =31 μM) was weaker than that of WT K-Ras (K_d = 10 μM). This suggests that the G12V mutant of K-Ras, which is one of the most frequently observed somatic Ras mutations in cancers, is compromised in its ability to bind Sos at the allosteric site and activate it, compared to wild-type.

Monitoring signal perturbations in W729E mutant Sos^{Cat} upon K-RasG12V•GTPγS binding. To characterize the binding of Ras•GTP at the catalytic site in the absence of allosteric activation of Sos, the allosteric site binding can be impaired through mutation of Trp729 of Sos^{Cat} to Glu (W729E) (11). Upon addition of unlabeled H-Ras•GTPγS to [^{13}C-methyl-M,I]-Sos^{Cat}W729E no perturbations were observed for any of the characteristic signals, including M726$^{(a)}$, M714$^{(a)/(c)}$ and M824$^{(c)}$, even when over titrated (Figure 6F), suggesting that there is no detectable binding to either of the binding sites. The fluorescence measurements for this interaction revealed a macroscopic K_d of 28 μM (Table 1), which may have been dominated by residual non-optimal binding to the sites away from the reporter residues used in the NMR. This value is comparable with the K_d of 32 μM obtained from fluorescence measurements for the interaction between Sos^{Cat}W729E and H-RasY64A•GTPγS, a combination of mutants which are supposed to block interactions at both allosteric and catalytic sites. The NMR data overall confirm that the

W729E mutation inhibits interaction with Ras•GTP at the allosteric site, preventing Sos activation and further binding of Ras•GTP at the catalytic site.

DISCUSSION

In our fluorescence-based studies we have monitored the intrinsic fluorescence of natively occurring Trp residues in Sos^{Cat} and $Sos^{HD\text{-}DH\text{-}PH\text{-}Cat}$ upon addition of Ras which is devoid of fluorophores, to avoid any possibility of perturbing protein structure or binding activity, as may be otherwise expected from using extrinsic dyes (16). As an orthogonal and complementary approach, we have also used NMR to report on the details of Ras and Sos interactions from the viewpoints of both interacting partners, in a site-specific manner. Using ^{13}C-methyl NMR probes for monitoring changes in structure and dynamics is innately non-perturbative and therefore highly robust (34,36-38). We identified three useful Sos^{Cat} methyl groups in $M726^{(a)}$, $M824^{(c)}$ and $M714^{(a)/(c)}$, which can be conveniently detected in well-resolved ^{1}H,^{13}C-HMQC spectra, and which report from allosteric and catalytic sites, as well as from the interface between them. These signals are sensitive to all aspects (structural as well as dynamic) of Ras-Sos interaction, and can be used for exploring mechanistic aspects of Sos function in various complexes. This strategy, applied consistently to a variety of combinations of different Ras isoforms (K-Ras, H-Ras and their selected mutants) in different nucleotide-loaded states (nucleotide-free, GDP-loaded, or loaded with GTP analogues) and different Sos constructs ($Sos^{HD\text{-}DH\text{-}PH\text{-}Cat}$, Sos^{Cat} and its mutants), allowed us to obtain for the first time site-specific information on the localized binding events at the allosteric and catalytic sites of Sos.

Taken together, our results are presented schematically as shown in Figure 8. The nucleotide-free form of H-Ras (which is not a species that is significantly populated in isolation *in vivo*, but may usefully represent a transition state) binds at the catalytic site only, affecting only the specific reporter signal $M824^{(c)}$ (Figure 8A). Note, in this interaction Sos is not activated due to the lack of allosteric site binding. The catalytic site binding also leads to significant signal perturbations in $H\text{-}Ras^{NF}$ itself. These results agree with crystallography studies where $H\text{-}Ras^{NF}$ has only ever been found at the catalytic site of Sos (8,10). Binding of GDP-loaded H-Ras to the catalytic site of non-activated Sos^{Cat} appears to be much weaker than that of Ras^{NF} (Figure 8B, Table 1), as judged by signal perturbations on Sos^{Cat} and Ras. Importantly, the NMR data suggest that H-Ras•GDP cannot bind at the allosteric site strongly enough to achieve significant activation of Sos; this is in agreement with previous observations (11) but also suggests that the level of Sos activation by Ras•GDP in the recent single-molecule studies (13) may have been overestimated. Weak transient binding of Ras•GDP at the catalytic site (even without activation) however would explain the modest homonucleotide GDP*→GDP exchange routinely observed in nucleotide release assays (10,11,13).

As expected, H-Ras•GTPγS was found to interact strongly with the allosteric site of Sos^{Cat} (Figure 8C), inducing strong signal shifts. Unexpectedly, binding of H-Ras•GTPγS at the catalytic site of fully-activated Sos^{Cat} was only weak and transient. This is in agreement with the result from saturating the allosteric site with H-RasY64A•GTPγS, a mutant which only binds at the allosteric site (11,12), and measuring H-Ras•GTPγS affinity at the catalytic site using fluorescence. The estimated lower limit of K_d value (≥21 μM) for Ras•GTPγS binding to the catalytic site of activated Sos is significantly higher than the K_d of H-Ras•GDP at the same site (1.9 μM) (11). Having a high affinity for Ras•GDP, which is the natural substrate for the catalytic reaction, and low affinity for Ras•GTP, which is the natural reaction product, provides a previously underappreciated preferred direction for the nucleotide exchange reaction, GDP→GTP. In a situation when both GDP and GTP are present in solution (eg, in cytosol), activated Sos would be preferentially recognizing Ras•GDP molecules with its catalytic site: once the exchange for GTP is complete, Ras•GTP would be released due to its lower affinity. To our knowledge, this is the first suggestion that the native nucleotide exchange mediated by Sos can have a preferred directionality, and is not just a passive re-loading of Ras molecules with a nucleotide according to the GTP/GDP ratio present in solution (3).

The NMR mapping experiments performed with K-Ras revealed results similar to H-Ras (Figure 8D), although for K-Ras the slow

exchange at the catalytic site was not detected, and overall binding was weaker (Table 1). The binding of H-Ras and K-Ras to Sos may therefore be subtly different in terms of dynamics and affinity, despite structural similarities, and very similar nucleotide exchange and hydrolysis properties (39). Interestingly, the mutation G12V of K-Ras showed substantially reduced binding to Sos (Table 1). Unlike the WT, the mutant lacks the ability to induce strong signal perturbations at the allosteric site of Sos, and only weakly binds at allosteric and catalytic sites (Figure 8E). Therefore, the G12V mutant is likely to be defective in its ability to bind Sos and activate it via allosteric site binding. Finally, the W729E mutant of Sos^{Cat}, which is known to block the interaction with Ras•GTP at the allosteric site (11), did not show any signal perturbations, neither at the allosteric or catalytic sites upon addition of H-Ras•GTPγS (Figure 8F), which confirms that in solution binding of Ras•GTP at the allosteric site is absolutely required to induce binding of Ras•GTP at the catalytic site. Similar results were also obtained for $Sos^{HD\text{-}DH\text{-}PH\text{-}Cat}$ construct (Table 1), which sterically occludes the allosteric site.

The low-affinity binding of Ras•GTP to the catalytic site of Sos highlighted in this study may have implications on how nucleotide exchange assays mediated by Sos are run and interpreted. The main scenarios of nucleotide exchange, together with the consequences of binding at each individual site, are presented in Figure 9. For simplicity, additional downregulation of Ras by N-terminal domains of Sos occluding the allosteric site (14) is omitted. Whereas scenario A represents early events in Sos activation and promoting GDP→GTP exchange on Ras, scenario B is expected to represent the native, functional GDP→GTP exchange which should be the fastest and the most efficient. It relies on strong binding of Ras•GTP to the allosteric site activating Sos, strong binding of Ras•GDP (the substrate) to the catalytic site, and fast release of Ras•GTP (the product) from the catalytic site once the exchange there is complete. A number of studies conducted some assays in these conditions (17,32,40-42). However, some nucleotide release assays quantified homonucleotide exchange as a measure of Sos activity, and followed scenarios C-E, with each of those suffering from one or several bottleneck interactions (see Figure 9) expected to slow down the apparent rate of nucleotide release or exchange. In these cases, the activity of Sos as measured by homonucleotide GDP→GDP or GTP→GTP exchange rates (10,11,13,40,43) may be underestimated. Recently, very high heteronucleotide GDP→GTP exchange rates of 0.28 s^{-1} were reported in the bulk assays which used non-modified nucleotides and biosensor detection (41): the S-shape of time courses (Fig. 4A in reference (41)) is consistent with the initial low-level activation quickly followed by the full activation, as is expected from combined scenarios A and B. Membrane tethering of Ras was shown to increase the rate of nucleotide exchange ca 500-fold compared with the bulk assays (32), but interestingly, the experiments done by these authors also reveal that the rate of heteronucleotide GDP→GTP exchange reaction is further ca 10 times faster than homonucleotide GDP→GDP in the identical conditions, reaching rate of ca 5 s^{-1} (Suppl. Fig. 2 in reference (32)). Even when Sos was activated by the presence of RasY64A loaded with a stable GTP analog, the homonucleotide exchange reaction rate was much lower (32). The marked increase in the rates for heteronucleotide exchange was also consistently observed in the presence of the N-terminal segment of Sos which downregulates its activity (32). In another bulk assay study (40), the rates of Sos^{Cat} catalyzed reactions for mantGDP→GTP and mantGTP→GTP exchanges were measured. In their study, addition of equimolar Sos^{Cat} to WT Ras increased the rates of exchange (relative to the intrinsic rates) by factors of 112 and 21, respectively, showing that fully-activated Sos^{Cat} enhances the rate of the heteronucleotide exchange reaction about five times faster than the rate of the homonucleotide GTP→GTP exchange reaction (Table II of reference (40)). This consistent increase of observed rates for native heteronucleotide exchange in various previous experiments can now be explained by the constructive combination of the stronger (ca tenfold) binding and activation of Sos by Ras•GTP (compared to Ras•GDP) at the allosteric site (11) and the at least tenfold greater binding affinity of the catalytic site for Ras•GDP (compared to Ras•GTP), which was revealed in this study. Thus, our results and a re-evaluation of previously published data, suggest that an adequate representation of the nucleotide exchange

catalyzed by Sos in assays may need to preferably measure the GDP→GTP exchange reaction, and be conducted in the presence of both Ras•GTP (to activate Sos) and Ras•GDP (as the native substrate for the catalytic conversion to Ras•GTP), and in the presence of an excess of GTP or its analog.

In conclusion, from our NMR Ras:Sos interaction assay developed and presented here, and experiments on different Ras forms, we were able to disentangle nucleotide-dependent Ras binding at the allosteric and catalytic sites of Sos. To achieve a fully functional heterotrimeric complex with Sos, e.g. to study its functioning mechanism, both GDP and GTP-loaded Ras molecules should be present. Our solution studies fully support previously proposed mechanism for positive feedback activation of Sos (10), but also suggest that the extent of such activation may have been previously underestimated, when the homonucleotide exchange rate was measured. The NMR approach described here opens new avenues through which to investigate this complex process directly in more detail in the future. Similarly, further NMR experiments can shed light on the molecular-level structural and dynamic detail of the processes involved in self-activating Sos by Ras (13). The site-specific interaction assay presented here may also aid the development and screening of future drugs designed against Ras:Sos interactions at particular sites of Sos (44).

Acknowledgements: We are grateful to Dr Matthew Cliff for useful program scripts for analysis of NMR signal shifts.

Conflict of interest: The Authors declare that they have no conflicts of interest with the contents of this article.

Author contributions: KJE, APG and ALB conceived and designed the project. UV, NV, LF, RB performed experiments and contributed materials. UV, APG and KJE wrote the manuscript. All authors contributed to the final manuscript.

REREFENCES

1. Pylayeva-Gupta, Y., Grabocka, E., and Bar-Sagi, D. (2011) RAS oncogenes: weaving a tumorigenic web. *Nat Rev Cancer* **11**, 761-774
2. Bourne, H. R., Sanders, D. A., and McCormick, F. (1990) The GTPase superfamily: a conserved switch for diverse cell functions. *Nature* **348**, 125-132
3. Buday, L., and Downward, J. (2008) Many faces of Ras activation. *Biochim Biophys Acta* **1786**, 178-187
4. Downward, J. (2003) Targeting RAS signalling pathways in cancer therapy. *Nat Rev Cancer* **3**, 11-22
5. Karapetis, C. S., Khambata-Ford, S., Jonker, D. J., O'Callaghan, C. J., Tu, D., Tebbutt, N. C., Simes, R. J., Chalchal, H., Shapiro, J. D., Robitaille, S., Price, T. J., Shepherd, L., Au, H. J., Langer, C., Moore, M. J., and Zalcberg, J. R. (2008) K-ras mutations and benefit from cetuximab in advanced colorectal cancer. *N Engl J Med* **359**, 1757-1765
6. Tan, C., and Du, X. (2012) KRAS mutation testing in metastatic colorectal cancer. *World J Gastroenterol* **18**, 5171-5180
7. Cox, A. D., Fesik, S. W., Kimmelman, A. C., Luo, J., and Der, C. J. (2014) Drugging the undruggable RAS: Mission possible? *Nat Rev Drug Discov* **13**, 828-851
8. Boriack-Sjodin, P. A., Margarit, S. M., Bar-Sagi, D., and Kuriyan, J. (1998) The structural basis of the activation of Ras by Sos. *Nature* **394**, 337-343

9. Rojas, J. M., Oliva, J. L., and Santos, E. (2011) Mammalian son of sevenless Guanine nucleotide exchange factors: old concepts and new perspectives. *Genes Cancer* **2**, 298-305
10. Margarit, S. M., Sondermann, H., Hall, B. E., Nagar, B., Hoelz, A., Pirruccello, M., Bar-Sagi, D., and Kuriyan, J. (2003) Structural evidence for feedback activation by Ras.GTP of the Ras-specific nucleotide exchange factor SOS. *Cell* **112**, 685-695
11. Sondermann, H., Soisson, S. M., Boykevisch, S., Yang, S. S., Bar-Sagi, D., and Kuriyan, J. (2004) Structural analysis of autoinhibition in the Ras activator Son of sevenless. *Cell* **119**, 393-405
12. Freedman, T. S., Sondermann, H., Friedland, G. D., Kortemme, T., Bar-Sagi, D., Marqusee, S., and Kuriyan, J. (2006) A Ras-induced conformational switch in the Ras activator Son of sevenless. *Proc Natl Acad Sci U S A* **103**, 16692-16697
13. Iversen, L., Tu, H.-L., Lin, W.-C., Christensen, S. M., Abel, S. M., Iwig, J., Wu, H.-J., Gureasko, J., Rhodes, C., Petit, R. S., Hansen, S. D., Thill, P., Yu, C.-H., Stamou, D., Chakraborty, A. K., Kuriyan, J., and Groves, J. T. (2014) Ras activation by SOS: Allosteric regulation by altered fluctuation dynamics. *Science* **345**, 50-54
14. Gureasko, J., Galush, W. J., Boykevisch, S., Sondermann, H., Bar-Sagi, D., Groves, J. T., and Kuriyan, J. (2008) Membrane-dependent signal integration by the Ras activator Son of sevenless. *Nat Struct Mol Biol* **15**, 452-461
15. Lenzen, C., Cool, R. H., Prinz, H., Kuhlmann, J., and Wittinghofer, A. (1998) Kinetic analysis by fluorescence of the interaction between Ras and the catalytic domain of the guanine nucleotide exchange factor Cdc25Mm. *Biochemistry* **37**, 7420-7430
16. Mazhab-Jafari, M. T., Marshall, C. B., Smith, M., Gasmi-Seabrook, G. M., Stambolic, V., Rottapel, R., Neel, B. G., and Ikura, M. (2010) Real-time NMR study of three small GTPases reveals that fluorescent 2'(3')-O-(N-methylanthraniloyl)-tagged nucleotides alter hydrolysis and exchange kinetics. *J Biol Chem* **285**, 5132-5136
17. Smith, M. J., Neel, B. G., and Ikura, M. (2013) NMR-based functional profiling of RASopathies and oncogenic RAS mutations. *Proc Natl Acad Sci U S A* **110**, 4574-4579
18. Shah, B. H., and Catt, K. J. (2004) GPCR-mediated transactivation of RTKs in the CNS: mechanisms and consequences. *Trends Neurosci* **27**, 48-53
19. Bondeva, T., Balla, A., Varnai, P., and Balla, T. (2002) Structural determinants of Ras-Raf interaction analyzed in live cells. *Mol Biol Cell* **13**, 2323-2333
20. Williams, J. G., Drugan, J. K., Yi, G. S., Clark, G. J., Der, C. J., and Campbell, S. L. (2000) Elucidation of binding determinants and functional consequences of Ras/Raf-cysteine-rich domain interactions. *J Biol Chem* **275**, 22172-22179
21. Spoerner, M., Herrmann, C., Vetter, I. R., Kalbitzer, H. R., and Wittinghofer, A. (2001) Dynamic properties of the Ras switch I region and its importance for binding to effectors. *Proc Natl Acad Sci U S A* **98**, 4944-4949
22. Spoerner, M., Hozsa, C., Poetzl, J. A., Reiss, K., Ganser, P., Geyer, M., and Kalbitzer, H. R. (2010) Conformational states of human rat sarcoma (Ras) protein complexed with its natural ligand GTP and their role for effector interaction and GTP hydrolysis. *J Biol Chem* **285**, 39768-39778
23. Ito, Y., Yamasaki, K., Iwahara, J., Terada, T., Kamiya, A., Shirouzu, M., Muto, Y., Kawai, G., Yokoyama, S., Laue, E. D., Walchli, M., Shibata, T., Nishimura, S., and Miyazawa, T. (1997) Regional polysterism in the GTP-bound form of the human c-Ha-Ras protein. *Biochemistry* **36**, 9109-9119
24. Araki, M., Shima, F., Yoshikawa, Y., Muraoka, S., Ijiri, Y., Nagahara, Y., Shirono, T., Kataoka, T., and Tamura, A. (2011) Solution structure of the state 1 conformer of GTP-bound H-Ras protein and distinct dynamic properties between the state 1 and state 2 conformers. *J Biol Chem* **286**, 39644-39653

25. Spoerner, M., Nuehs, A., Herrmann, C., Steiner, G., and Kalbitzer, H. R. (2007) Slow conformational dynamics of the guanine nucleotide-binding protein Ras complexed with the GTP analogue GTPgammaS. *FEBS J* **274**, 1419-1433
26. Sprangers, R., and Kay, L. E. (2007) Quantitative dynamics and binding studies of the 20S proteasome by NMR. *Nature* **445**, 618-622
27. Vo, U., Embrey, K. J., Breeze, A. L., and Golovanov, A. P. (2013) (1)H, (13)C and (15)N resonance assignment for the human K-Ras at physiological pH. *Biomol NMR Assign* **7**, 215-219
28. Golovanov, A. P., Hautbergue, G. M., Wilson, S. A., and Lian, L. Y. (2004) A simple method for improving protein solubility and long-term stability. *J Am Chem Soc* **126**, 8933-8939
29. Johnson, B. A., and Blevins, R. A. (1994) NMR View: A computer program for the visualization and analysis of NMR data. *J Biomol NMR* **4**, 603-614
30. Leatherbarrow, R. J. (1992) GraFit version 3.0. Data Analysis and Graphics program for the IBM PC. Erithacus Software
31. Mou, T. C., Gille, A., Fancy, D. A., Seifert, R., and Sprang, S. R. (2005) Structural basis for the inhibition of mammalian membrane adenylyl cyclase by 2 '(3')-O-(N-Methylanthraniloyl)-guanosine 5 '-triphosphate. *J Biol Chem* **280**, 7253-7261
32. Gureasko, J., Kuchment, O., Makino, D. L., Sondermann, H., Bar-Sagi, D., and Kuriyan, J. (2010) Role of the histone domain in the autoinhibition and activation of the Ras activator Son of Sevenless. *Proc Natl Acad Sci U S A* **107**, 3430-3435
33. Sondermann, H., Nagar, B., Bar-Sagi, D., and Kuriyan, J. (2005) Computational docking and solution x-ray scattering predict a membrane-interacting role for the histone domain of the Ras activator son of sevenless. *Proc Natl Acad Sci U S A* **102**, 16632-16637
34. Stoffregen, M. C., Schwer, M. M., Renschler, F. A., and Wiesner, S. (2012) Methionine scanning as an NMR tool for detecting and analyzing biomolecular interaction surfaces. *Structure* **20**, 573-581
35. Kovrigin, E. L. (2012) NMR line shapes and multi-state binding equilibria. *J Biomol NMR* **53**, 257-270
36. Mas, G., Crublet, E., Hamelin, O., Gans, P., and Boisbouvier, J. (2013) Specific labeling and assignment strategies of valine methyl groups for NMR studies of high molecular weight proteins. *J Biomol NMR* **57**, 251-262
37. Gelis, I., Bonvin, A. M., Keramisanou, D., Koukaki, M., Gouridis, G., Karamanou, S., Economou, A., and Kalodimos, C. G. (2007) Structural basis for signal-sequence recognition by the translocase motor SecA as determined by NMR. *Cell* **131**, 756-769
38. Krishnarjuna, B., Jaipuria, G., Thakur, A., D'Silva, P., and Atreya, H. S. (2011) Amino acid selective unlabeling for sequence specific resonance assignments in proteins. *J Biomol NMR* **49**, 39-51
39. Quinlan, M. P., Quatela, S. E., Philips, M. R., and Settleman, J. (2008) Activated Kras, but not Hras or Nras, may initiate tumors of endodermal origin via stem cell expansion. *Mol Cell Biol* **28**, 2659-2674
40. Ford, B., Skowronek, K., Boykevisch, S., Bar-Sagi, D., and Nassar, N. (2005) Structure of the G60A mutant of Ras: implications for the dominant negative effect. *J Biol Chem* **280**, 25697-25705
41. Kunzelmann, S., and Webb, M. R. (2011) Fluorescence detection of GDP in real time with the reagentless biosensor rhodamine-ParM. *Biochem J* **440**, 43-49
42. Burns, M. C., Sun, Q., Daniels, R. N., Camper, D., Kennedy, J. P., Phan, J., Olejniczak, E. T., Lee, T., Waterson, A. G., Rossanese, O. W., and Fesik, S. W. (2014) Approach for targeting Ras with small molecules that activate SOS-mediated nucleotide exchange. *Proc Natl Acad Sci U S A* **111**, 3401-3406
43. Hall, B. E., Yang, S. S., Boriack-Sjodin, P. A., Kuriyan, J., and Bar-Sagi, D. (2001) Structure-based mutagenesis reveals distinct functions for Ras switch 1 and switch 2 in Sos-catalyzed guanine nucleotide exchange. *J Biol Chem* **276**, 27629-27637

44. Winter, J. J., Anderson, M., Blades, K., Brassington, C., Breeze, A. L., Chresta, C., Embrey, K., Fairley, G., Faulder, P., Finlay, M. R., Kettle, J. G., Nowak, T., Overman, R., Patel, S. J., Perkins, P., Spadola, L., Tart, J., Tucker, J. A., and Wrigley, G. (2015) Small molecule binding sites on the Ras:SOS complex can be exploited for inhibition of Ras activation. *J Med Chem* **58**, 2265-2274

FOOTNOTES

UV and this work were supported by the Medical Research Council Industrial CASE Studentship G1000399-3/1 (awarded to APG and KJE).

The abbreviations used are:
GAP, guanine nucleotide activating factor; GEF, guanine nucleotide exchange factor; HMQC, heteronuclear multiple quantum coherence; Ras^{NF}, nucleotide-free form of Ras; Sos, Son of Sevenless; TROSY, transverse optimized spectroscopy; WT, wild type.

FIGURE LEGENDS

FIGURE 1. Change in intrinsic fluorescence signal of Sos^{Cat} variants upon addition of protein ligands, used to determine the dissociation constants K_d presented in Table 1. Individual panels show binding of WT Sos^{Cat} with (A) H-Ras•GDP; (B) H-Ras•GTPγS; (C) H-Ras•GppNp; (D) H-Ras•GppCp; (E) H-RasY64A•GTPγS; (F) Binding of Sos^{Cat}W729E with H-Ras•GTPγS; (G) $Sos^{HD\text{-}DH\text{-}PH\text{-}Cat}$ with H-Ras•GTPγS; (H) Sos^{Cat}W729E with H-RasY64A•GTPγS; (I) Sos^{Cat}W729E with H-Ras•GDP; (J) WT Sos^{Cat} (pre-loaded with 30 μM H-RasY64A•GTPγS) with H-Ras•GTPγS; (K) WT Sos^{Cat} with K-Ras•GTPγS, and (L) WT Sos^{Cat} with K-RasG12V•GTPγS. The fluorescence data was fitted to a single-site binding model using GraFit software (30).

FIGURE 2. Differences between H-Ras states in the $^{1}H,^{15}N$-TROSY spectra. (A) Comparison between H-Ras•GDP (blue) and H-Ras^{NF} (red). (B) Comparison between H-Ras•GDP (blue) and H-Ras•GTPγS (pink). (C) the spectra of H-Ras bound to GDP (blue), H-Ras^{NF} (red) and H-Ras^{NF} bound to Sos (green) in a 2:1 Ras:Sos stoichiometry, (D) the spectra of H-Ras•GDP (blue) and H-Ras•GDP:Sos (green) in a 2:1 Ras:Sos stoichiometry. Spectra A-D were collected at 25 ºC. (E) At 18 °C, comparison between H-Ras•GDP (blue), H-Ras•GTPγS (magenta) and H-Ras•GTPγS bound to Sos (green) in a 2:1 Ras:Sos stoichiometry.

FIGURE 3. Overlay of a representative region of the $^{1}H,^{15}N$-TROSY spectra of different forms of ^{15}N-labeled H-Ras. (A) The spectra of H-Ras bound to GDP (blue), H-Ras^{NF} (red) and H-Ras^{NF} bound to Sos (green) in a 2:1 stoichiometry, recorded at 25 °C. (B) The spectra of H-Ras•GDP (blue) and H-Ras•GDP:Sos (green) in a 2:1 stoichiometry, recorded at 25 °C. (C) Comparison between H-Ras•GDP (blue), H-Ras•GTPγS (magenta), and H-Ras•GTPγS bound to Sos (green) in a 2:1 stoichiometry, recorded at 18 °C. Direction of, representative, signal shifts due to nucleotide change from GDP to GTPγS are marked with dashed black arrows. Direction of the shifts that are caused by the subsequent addition of Sos^{Cat} to H-Ras•GTPγS are marked with dashed red arrows. Spectrally aliased side chain resonances are labeled with asterisks.

FIGURE 4. Site-specific reporter signals of Sos. Expanded fingerprint regions of the $^{1}H,^{13}C$-HMQC spectra of 60 μM Sos showing: (A) region with assigned ^{13}C-methyl Met resonances apportioned to allosteric and catalytic sites, and (B) region showing non-assigned ^{13}C- methyl signals of Ile residues as additional reporter signals. (C) Position of selected Met residues (highlighted in green and labeled

individually) in relation to the Ras:Sos crystal structure (Pdb ID: 1NVV). Ras molecules bound at the allosteric and catalytic sites of Sos (grey) are shown in purple and orange, respectively. The superscripts (a) and (c) mark the proximity of Met residues to the allosteric and catalytic sites, respectively.

FIGURE 5. An example of using mutagenesis to assign methyl signals of Met in Sos^{Cat}, and relating Met positions to the structure. Overlays of ^{13}C-methyl region of ^{1}H,^{13}C-HMQC spectra for WT (blue) and mutants (red) M824A (A) and M726A (B) of Sos^{Cat}. Signals affected by the mutation are enclosed in boxes. Structures below show reporter groups of Sos in contact with residues of H-Ras. C) The structure of the catalytic interface, deduced from the crystal structure of $H\text{-}Ras^{NF}$ form. $H\text{-}Ras^{NF}$ (orange) bound at the catalytic site of Sos (blue). Residue $M824^{(c)}$ (green) forms hydrophobic interactions with H-Ras Y64 (cyan). D) $M726^{(a)}$ (highlighted in green) interacts with H-Ras at the allosteric site (purple). The figures were produced in PyMol.

FIGURE 6. Monitoring changes in the ^{1}H,^{13}C- HMQC spectra of Sos^{Cat} upon the addition of Ras. The Met methyl resonances of Sos^{Cat} (A-E) (red) and (F) Sos^{Cat}W729E (red) were monitored upon the addition of Ras at Ras:Sos stoichiometry of 0.5:1 (blue), 1:1 (green), 1.5:1 (orange), 2:1 (cyan), 3:1 (purple) and 4:1 (black) in the HMQC spectra. The titrated Ras form is (A) $H\text{-}Ras^{NF}$ (B) H-Ras•GDP, (C) H-Ras•GTPγS, (D) K-Ras•GTPγS, (E) K-RasG12V•GTPγS and F) H-Ras•GTPγS. Chemical shift perturbations and signal broadening are indicated as black boxes and dashed boxes, respectively. Characteristic states occurring for $M824^{(c)}$ signal upon addition of H-Ras•GTPγS are marked in the panel (C) as I, II and III.

FIGURE 7. Consequences of two-site binding and chemical exchange rates for NMR signal shifts and apparent binding constants. (A) Horizontal slices through the $M824^{(c)}$ cross-peak of Sos^{Cat} showing relative spectral changes in ^{1}H dimension upon addition of specified equivalents of H-Ras•GTPγS. The peak positions for the binding states I, II and III are marked. (B) The thermodynamic cycle for two-site binding reaction between receptor (R) and ligand (L) with plausible values of K_d and off-rates k_{off} used for simulation with LineShapeKin software (35). L_a and L_c denote ligands bound at the allosteric and catalytic sites, respectively, and binding states I, II and III are labelled accordingly. The simulated spectral traces (with [R] fixed at 60 μM) shown in panel (C) mimic qualitatively the behavior of experimental spectra presented in (A). State I corresponds to chemical shift of free Sos^{Cat}, state II to H-Ras•GTPγS bound tightly (in slow exchange) at the allosteric site, and state III to a second H-Ras•GTPγS molecule binding weakly (in fast exchange) at the catalytic site. The simulated dependence of the fraction of R bound vs the [L]/[R] ratio can, however, be easily fitted into a one-site binding isotherm (D) which yields an apparent "macroscopic" K_d value of ca. 5 μM; a value close to that measured for Sos^{Cat}:H-Ras•GTPγS binding using fluorescence (see Table 1).

FIGURE 8. Proposed modes of Ras binding to Sos from our NMR assay. (A) $H\text{-}Ras^{NF}$ binds at the catalytic site of Sos and perturbs residues $M824^{(c)}$ and $M714^{(a)/(c)}$ only (green dots). (B) H-Ras•GDP binding to the catalytic site only slightly perturbs Sos residues $M714^{(a)/(c)}$ and $M824^{(c)}$. Unperturbed signal from Sos $M726^{(a)}$ is indicated as a black dot. Double ended arrows indicate weak interactions. (C) H-Ras•GTPγS binds at the allosteric site of Sos, as confirmed by the perturbation of residue $M726^{(a)}$. The binding of H-Ras•GTPγS at the allosteric site induces a conformational change to Sos, detected by the perturbation of residues $M714^{(a)/(c)}$ and $M824^{(c)}$, which allows a second H-Ras•GTPγS to bind weakly to the catalytic site. (D) The mechanism is similar for K-Ras•GTPγS as for H-Ras•GTPγS (E) K-RasG12V•GTPγS binds to allosteric and catalytic sites only weakly. (F) No Ras binding was observed at both the allosteric and catalytic sites of Sos W729E mutant which blocks Ras binding to the allosteric site.

FIGURE 9. Common scenarios for nucleotide exchange regimes in Ras:Sos system. The allosteric site is schematically shown at the bottom of Sos, and catalytic at the top. For each scenario, the state of the system and qualitative description of binding is shown on the right, including the expected exchange

rate of the nucleotide which was initially bound to incoming Ras. Scenario A corresponds to initial low-level activation of Sos when no Ras•GTP is present yet, with GDP→GTP exchange driven by the excess of GTP over GDP in the cytosol. Once enough Ras•GTP molecules are produced, they lead to positive feedback activation of Sos (scenario B), where the affinity at the catalytic site is high for Ras•GDP and low for Ras•GTP, leading to efficient, native turnover and expected maximum GDP→GTP exchange rate. Both nucleotides (+GDP and +GTP) are present. In scenarios C-E, typical for assays where only one type of nucleotide is present in excess, a release of labeled nucleotide (marked with *) initially bound to the catalytic site is expected to be slowed down (relative to the native rate for Scenario B), due to either stalling of Sos recycling (Scenario C) or the presence of weak binding bottleneck steps at the allosteric (D), or catalytic sites (E).

TABLE 1. The summary of macroscopic dissociation constants for Ras:Sos complexes measured by fluorescence. Protein variants used for each titration experiment, as well as a brief description of the expected functional effect of mutation, are indicated.

Description of expected effect of mutation used	Sos variant present[1]	Ras variant added	Measured K_d (μM)
None	Sos^{Cat}	H-Ras·GDP	54 ±4
None	Sos^{Cat}	H-Ras·GTPγS	5.0 ± 0.8
None	Sos^{Cat}	H-Ras·GppNp	6.0 ± 0.9
None	Sos^{Cat}	H-Ras·GppCp	8.0 ± 1.0
Is not expected to bind at catalytic site	Sos^{Cat}	H-RasY64A·GTPγS	10 ± 1
Binding expected to be hindered at allosteric site	Sos^{Cat}W729E	H-Ras·GTPγS	28 ± 1
Binding expected to be hindered at allosteric site	$Sos^{HD\text{-}DH\text{-}PH\text{-}Cat}$	H-Ras·GTPγS	24 ± 2
Binding expected to be hindered at both sites of Sos	Sos^{Cat}W729E	H-RasY64A·GTPγS	32 ± 3
Binding expected to be hindered at allosteric site	Sos^{Cat}W729E	H-Ras·GDP	67 ± 2
HRasY64A•GTPγS expected to partially saturate allosteric site	Sos^{Cat} (pre-loaded with 30 μM HRasY64A·GTPγS)	H-Ras·GTPγS	21 ± 2 [2]
None	Sos^{Cat}	K-Ras·GTPγS	10 ± 1
Oncogenic variant	Sos^{Cat}	K-RasG12V·GTPγS	31 ± 2

[1] Unless stated otherwise, the WT version of protein was used.
[2] Lower limit estimate.

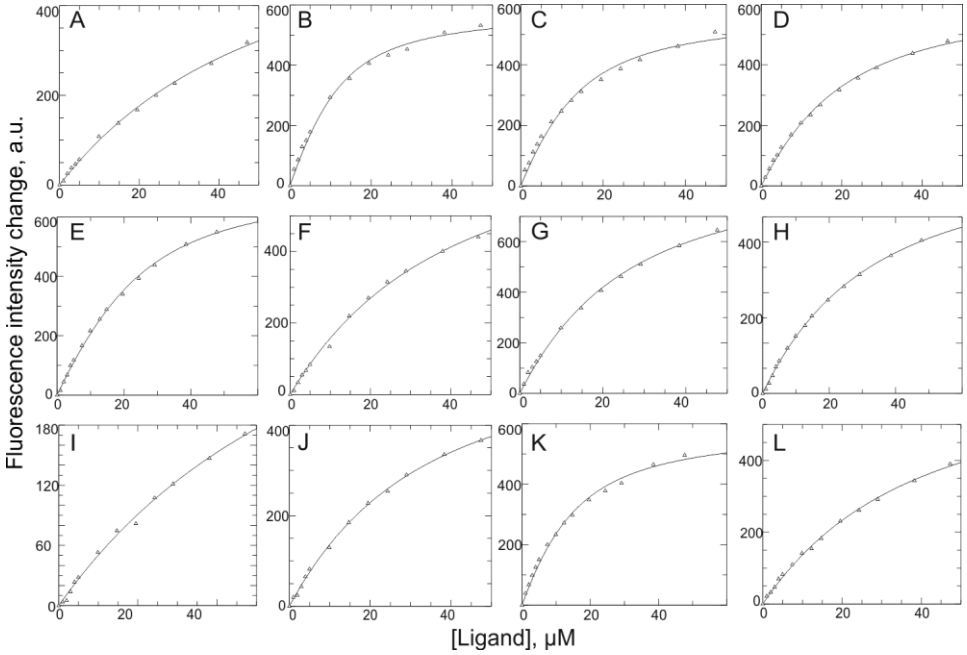

Figure 1.

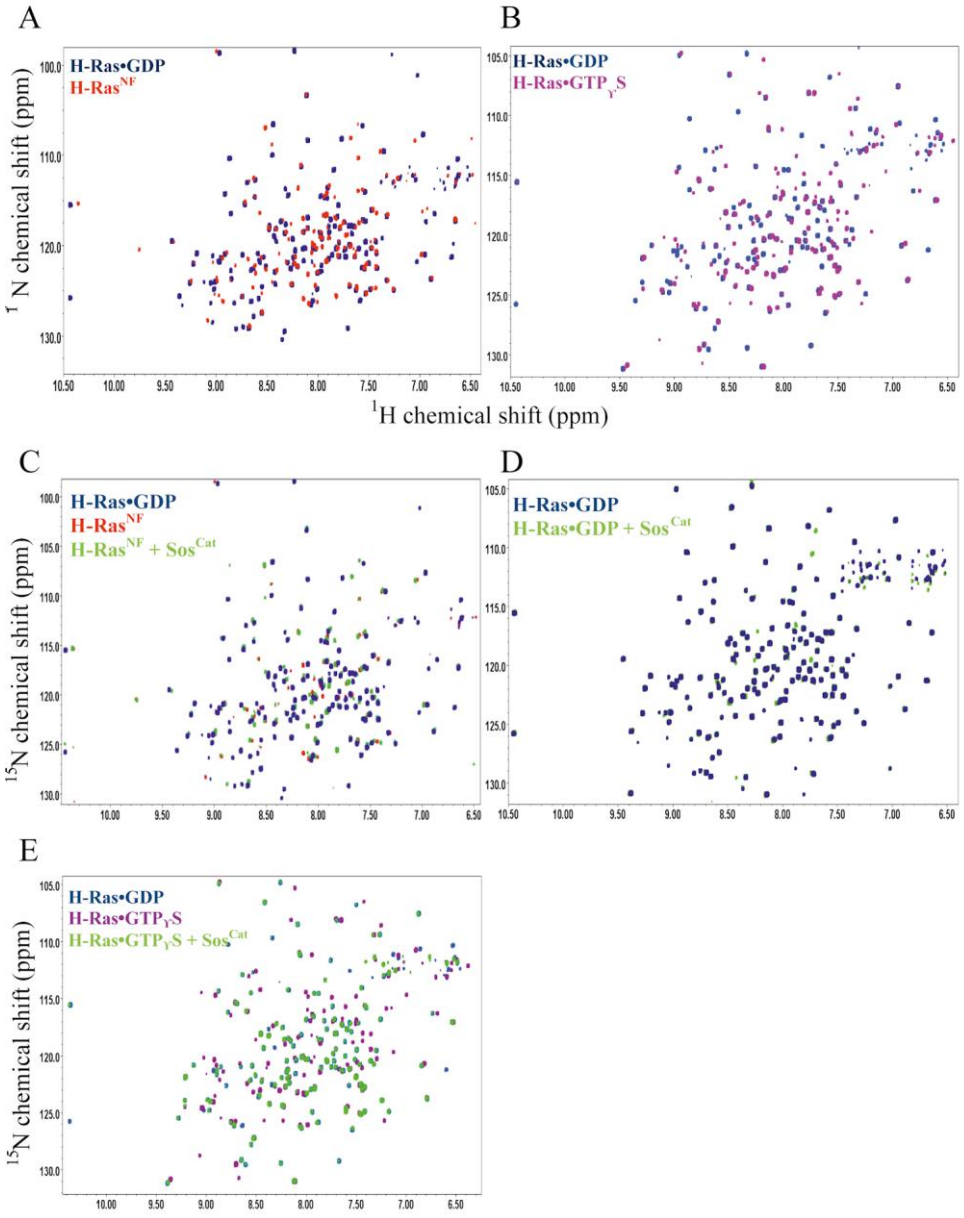

Figure 2.

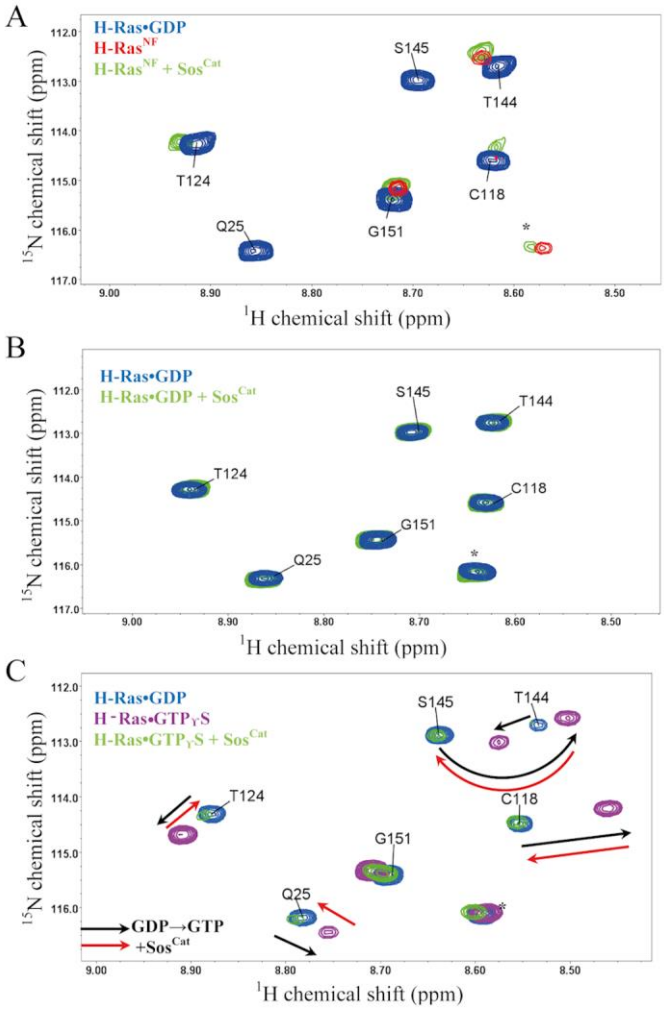

Figure 3.

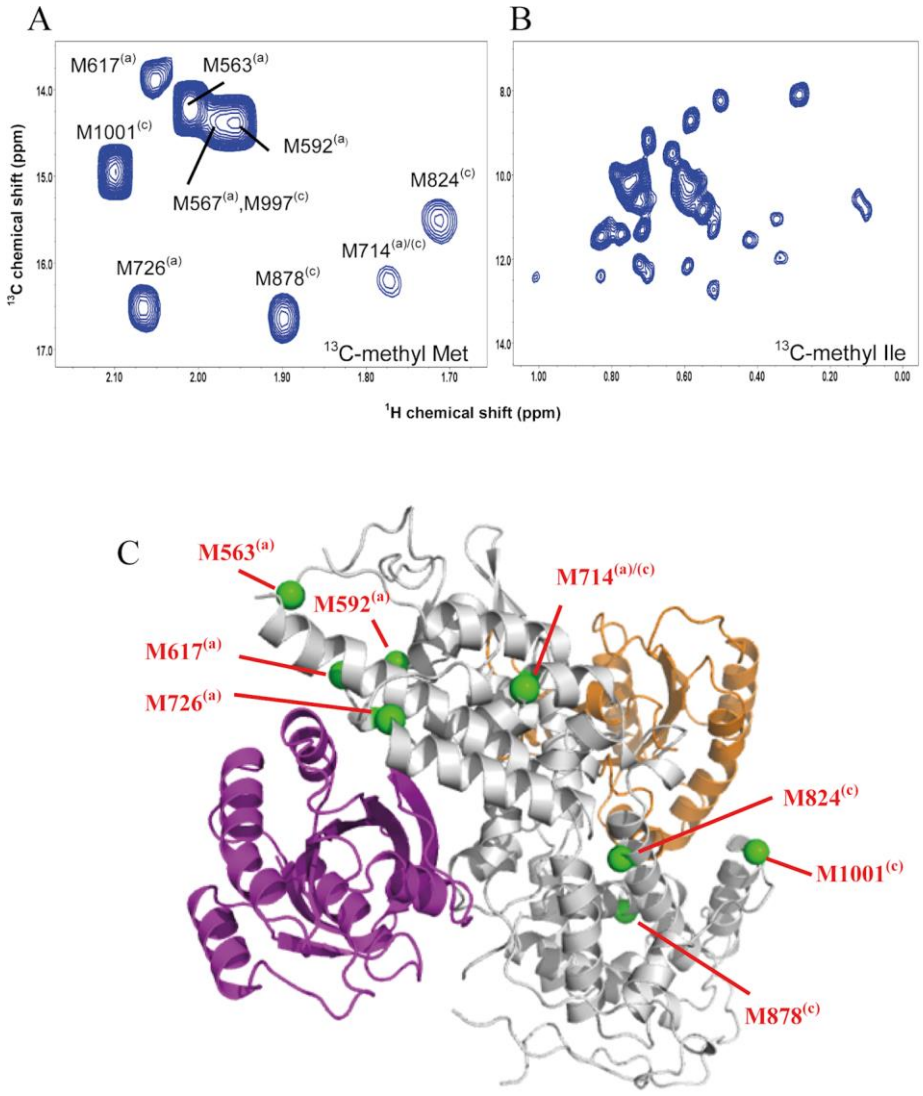

Figure 4.

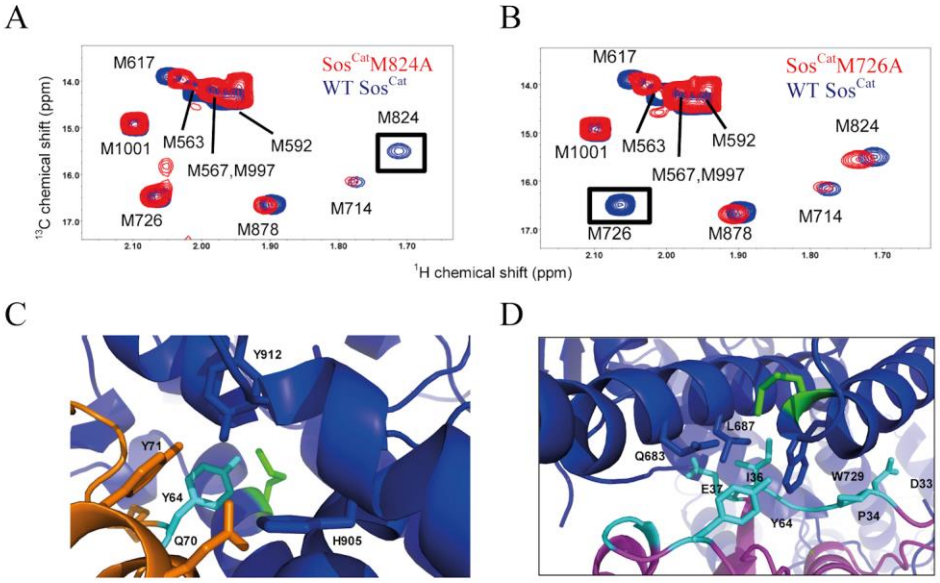

Figure 5.

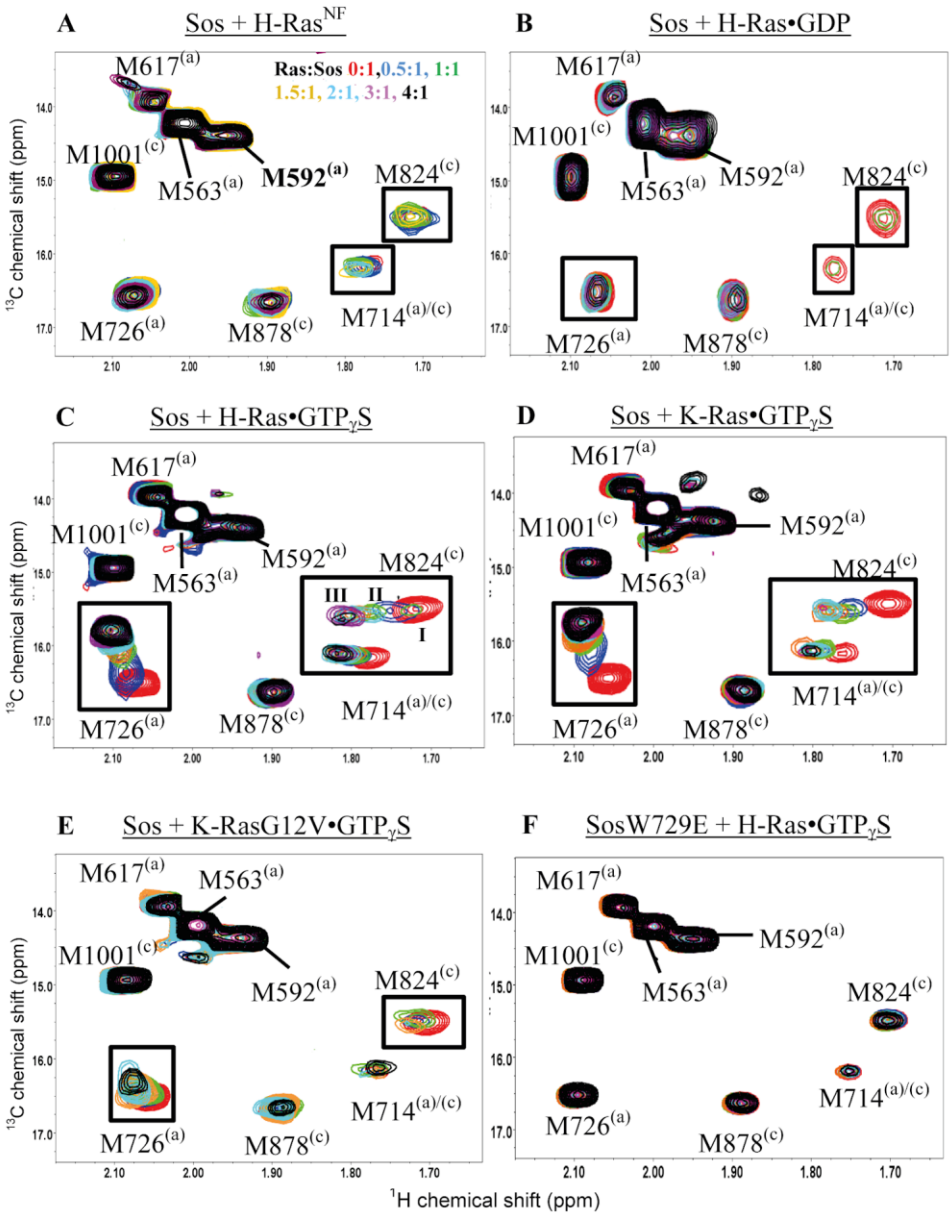

Figure 6.

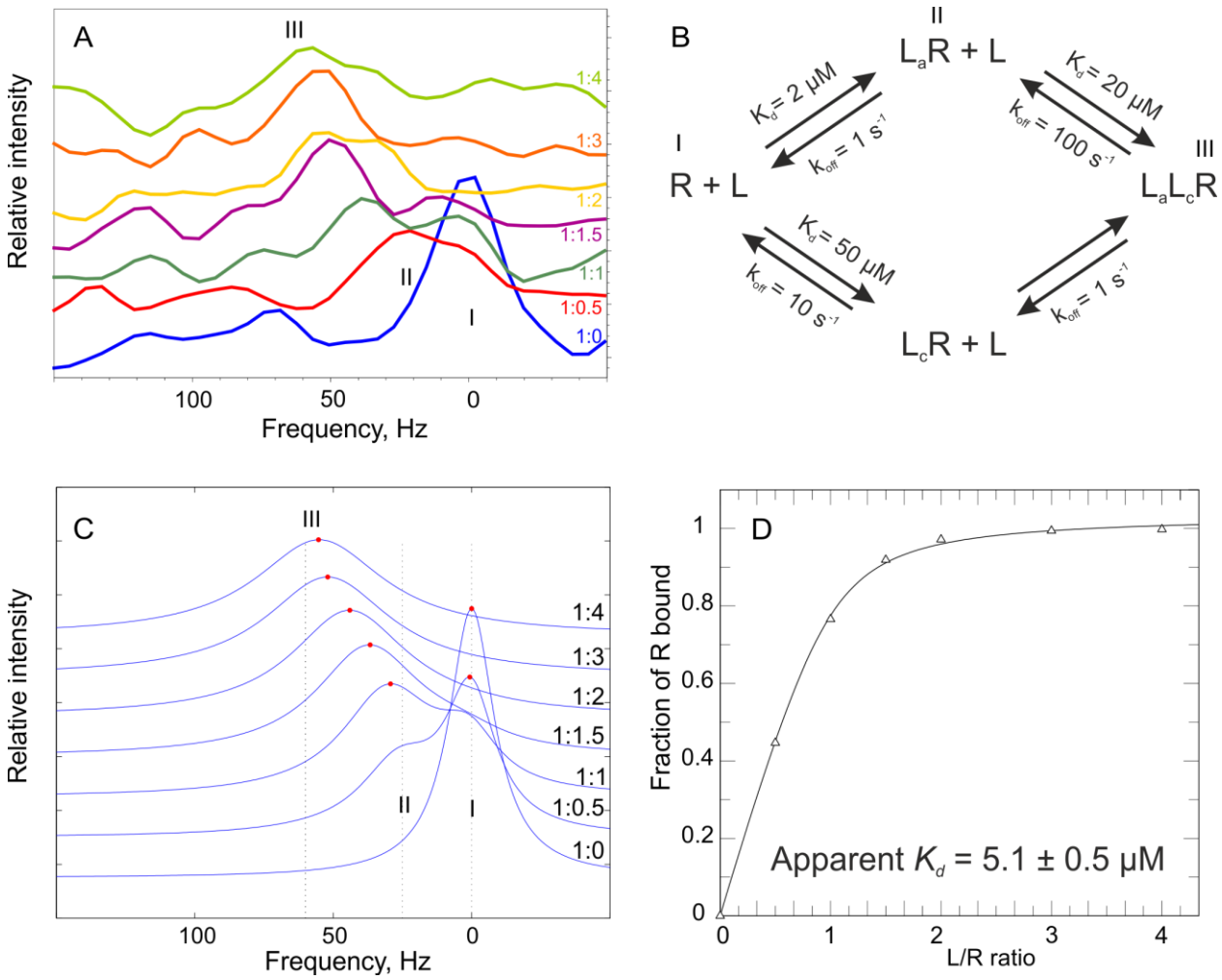

Figure 7.

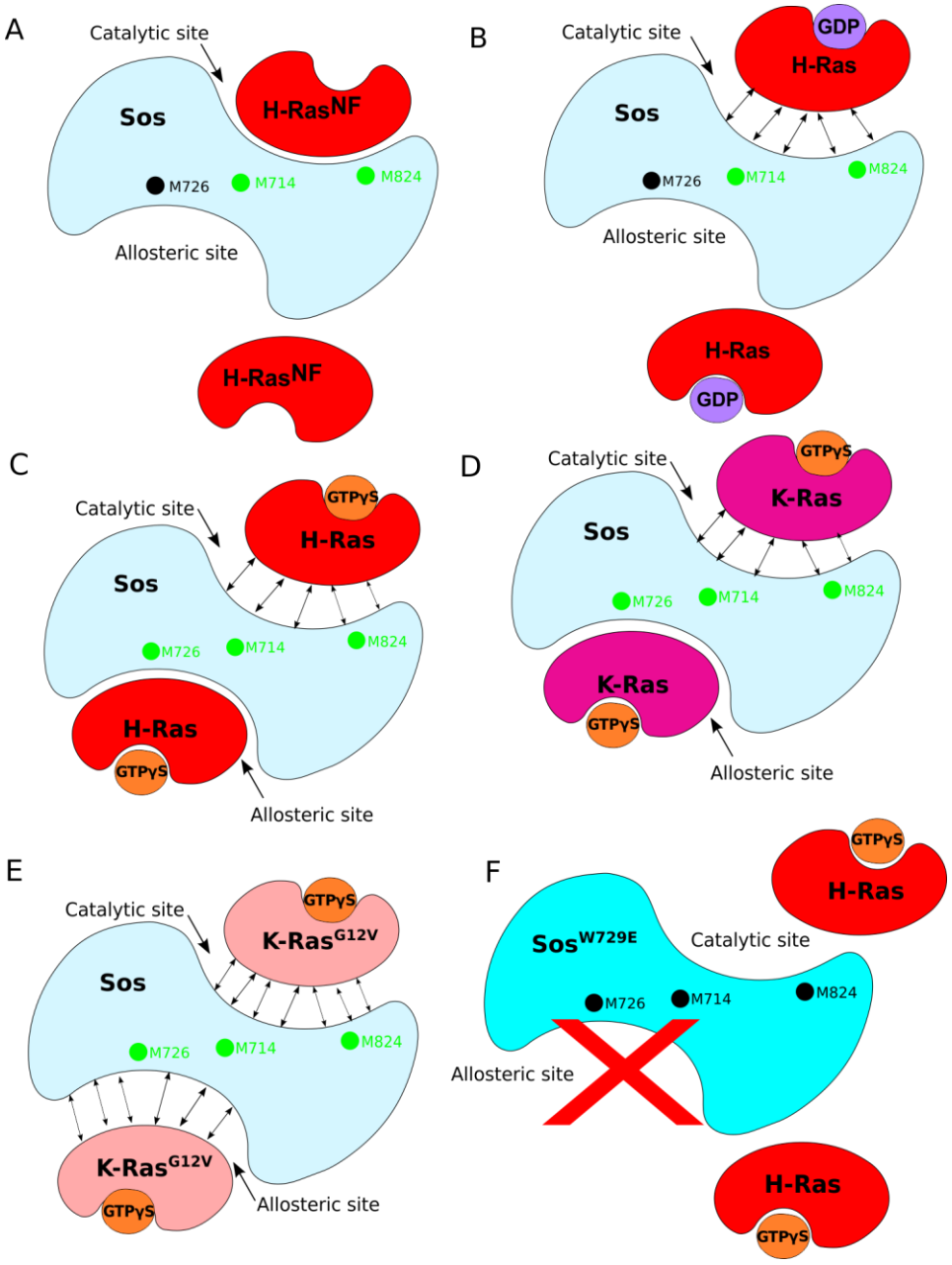

Figure 8.

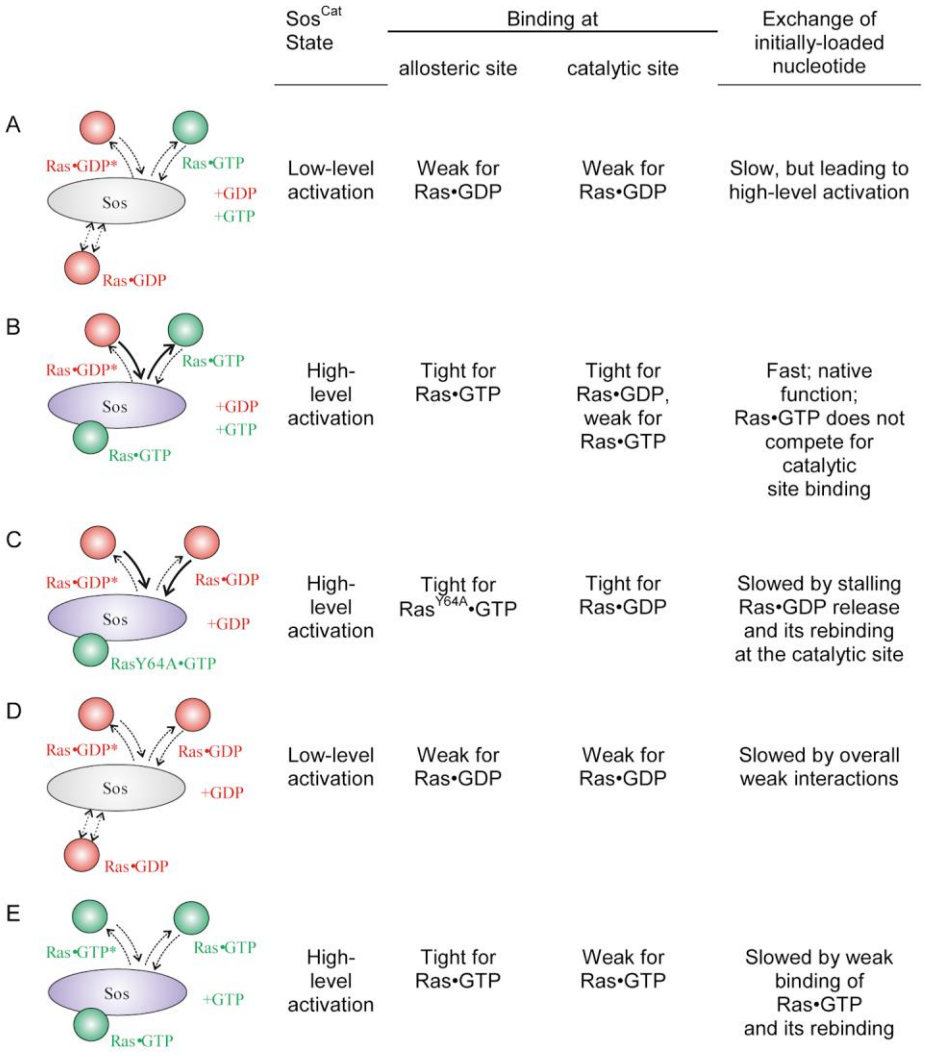

Figure 9.

Monitoring Ras Interactions with the Nucleotide Exchange Factor Sos using Site-specific NMR Reporter Signals and Intrinsic Fluorescence

Uybach Vo, Navratna Vajpai, Liz Flavell, Romel Bobby, Alexander L. Breeze, Kevin J. Embrey and Alexander P. Golovanov

J. Biol. Chem. published online November 12, 2015
